Microchimica Acta (2019) 186:593
https://doi.org/10.1007/s00604-019-3702-4

ORIGINAL PAPER

ZnO nanoparticles on MoS_2 microflowers for ultrasensitive SERS detection of bisphenol A

Yingnan Quan[1,2,3] · Jiacheng Yao[1,2,3] · Shuo Yang[4] · Lei Chen[1,2,3] · Jia Li[3] · Yang Liu[1,2,3] · Jihui Lang[1,2,3] · He Shen[1,2,3] · Yaxin Wang[1,2,3] · Yanyan Wang[3] · Jinghai Yang[1,2,3] · Ming Gao[1,2,3]

Received: 14 March 2019 / Accepted: 13 July 2019

Abstract

A heterojunction microcomposite was synthesized that consists of ZnO nanoparticles (ZnO NPs) anchored on MoS_2 microflowers (MoS_2 MFs). The material is shown to enable trace level detection of the pollutant bisphenol A (BPA). The microcomposite was characterized by XRD, XPS, SEM and TEM. In addition, coupling reaction between phenolic estrogens and Pauly's reagents was adopted to greatly enhance the SERS signal. BPA display a characteristic Raman band at 1592 cm^{-1} which can be used for its selective detection. The assay is highly sensitive and has a 1 nM detection limit which is the lowest among the reported semiconductor substrates.

Keywords MoS_2/ZnO MCs · MoS_2 MFs · SERS · Enhancement mechanism

Introduction

Bisphenol A (BPA) is an endocrine-disrupting chemical (EDC) that is widely found in the environment and food containers. Even if the levels of BPA entering the body are very low, it will disrupt the endocrine system and lead to cardiovascular and other diseases [1–3]. Therefore, a large number of technologies have been developed for the detection of BPA [4–6]. Recently, surface enhanced Raman scattering (SERS) technology has been widely used in biochemical assays due to its advantages such as low cost, high sensitivity and strong anti-interference ability [7–9]. Specially, SERS can be used to identify and quantify analytes of the trace-level molecules based on a single-molecule level. Therefore, the determination of trace BPA by SERS method is promising. The conventional SERS materials are based on noble metals, in which the Raman intensity can be enhanced by a factor of 10^6 or higher [10]. However, the development of noble metal substrate was limited by its low stability and poor biocompatibility [11]. For the sake of making up for the defects of metal, semiconductor material as candidate material has gradually become the research focus of SERS substrate.

Two-dimensional (2D) materials (e.g. MoS_2) has broad application prospects in the fields of optics and electronics owing to its excellent physicochemical properties and unique layered structures [12–14]. It has been found that MoS_2 can be promising candidates for the next-generation SERS substrates. However, the Raman enhancement factors and the limits of detection of MoS_2 are still greatly inferior to the noble metal structures [15]. Therefore, it is of vital significance to explore methods to improve the SERS activity of MoS_2. At present, combining MoS_2 with foreign atoms or molecules is an effective means to improve the sensing performance of MoS_2. Inspired by the exciting advantages of good stability, diverse structure and excellent sensing performance, ZnO was selected to combine with MoS_2 to form layered composite materials [16–18]. The combination of the two is expected to enhance the SERS activity of each component, becoming a promising SERS substrate material.

✉ Ming Gao
gaomingphy@126.com

[1] Key Laboratory of Functional Materials Physics and Chemistry of the Ministry of Education, Jilin Normal University, Changchun 130103, People's Republic of China

[2] National Demonstration Centre for Experimental Physics Education, Jilin Normal University, Siping 136000, People's Republic of China

[3] Key Laboratory of Preparation and Application of Environmental Friendly Materials, Ministry of Education, Jilin Normal University, Changchun 130103, People's Republic of China

[4] Changchun Institute of Optics, Fine Mechanics and Physics, Chinese Academy of Sciences, Changchun 130033, People's Republic of China

Published online: 01 August 2019

However, to the best of our knowledge, no previous study regarding the application of the MoS_2/ZnO composites as SERS substrate for trace BPA detection has not been reported to date.

In this work, a low-temperature hydrothermal method was used to combine MoS_2 (narrow-band gap p-type semiconductors) with ZnO (wide-band gap n-type semiconductors) to optimize the performance of each component. As SERS substrates, MoS_2/ZnO composites show properties of superior detection ability, which are ideal for detecting harmful molecules. This study provides a highly efficient method for developing noble-metal-free, highly-efficient, and stable MoS_2-based SERS substrate, which also shed light on a deep understanding about the charge-transfer based enhancement mechanism.

Experimental

Materials and apparatus

All chemical reagents in our experiment were of AR grade (SINOPHARM, CHINA) and no further purification. Ultrapure water was used in all experiments. Sodium molybdate ($Na_2MoO_4{\cdot}2H_2O$), thiourea (CH_4N_2S), citric acid monohydrate ($C_6H_8O_7{\cdot}H_2O$), zinc nitrate hexahydrate ($Zn(NO_3)_2{\cdot}6H_2O$) and BPA were bought from Aladdin Industrial Corporation (Shanghai, China. http://www.aladdin-e.com). Hexamethylenetetramine ($C_6H_{12}N_4$) and ammonia water (NH_3) were bought from Sinopharm group chemical reagent Co., Ltd. (Shanghai, China. http://www.sinoreagent.com.cn). Real water samples were taken from local tap water (Changchun, China).

The structure quality was characterized by X-ray diffraction (XRD, D/Max 3C, Rigaku, Japan, http://www.rigaku.com.cn) and X-ray photoelectron spectra (XPS, ESCALAB 250X, Thermo Scientific, USA, https://www.thermofisher.com.cn). The morphology of the samples was characterized by scanning electron microscopy (SEM, JSM-7800F, JEOL, Japan, http://www.jeol.com) and transmission electron microscope (TEM, JEM-2100HR, JEOL, Japan, http://www.jeol.com). The SERS signals were detected under a 514.5 nm Ar^+ ion laser (inVia Raman Microscope, Renishaw, UK, https://www.renishaw.com).

Preparation of MoS_2 microflowers (MoS_2 MFs)

Firstly, 500 mg $Na_2MoO_4{\cdot}2H_2O$ and 700 mg CH_4N_2S were mixed into 70 mL of distilled water and stirred for 30 min until completely dissolved. Whereafter, 500 mg of $C_6H_8O_7{\cdot}H_2O$ was added into the foregoing mixed liquid, stirred for 20 min and then diverted into a 100 mL Teflon lined stainless steel autoclave. Then the autoclave was sealed and heated at 240 °C for 24 h. After cooling to room temperature, the black precipitates were thoroughly rinsed with ethanol and double-distilled water and dried at 60 °C for 6 h.

Preparation of MoS_2/ZnO micron composites (MoS_2/ZnO MCs)

0.3720 g $Zn(NO_3)_2{\cdot}6H_2O$ and 0.0883 g $C_6H_{12}N_4$ were mixed and dissolved in 50 mL deionized water, 20 mg MoS_2 powders were well dispersed in the mixed solution by ultrasonication. Then, 2 mL of ammonia water (25~28%) was mixed into the abovementioned solution and put it into a 60 °C of water bath pot for 3 h. Then the gray-black precipitates were washed with deionized water and ethanol. Finally, the MoS_2/ZnO MCs solid powders were collected after drying at 60 °C for 6 h.

The SERS experiments of trace BPA

BPA was selected as the probe molecule for SERS analysis. Coupling reaction between phenolic estrogens and Pauly's reagents was adopted to enhance the adhesion of BPA to MoS_2/ZnO MCs substrate. Pauly's reagents (Reagent A: 4.5 g p-aminobenzene sulfonic acid powders were dissolved in 500 mL deionized water and 5 mL 12 M HCl solution was added. Reagent B: 5% sodium nitrite solution and reagent C: 10% sodium carbonate solution) are stored at 4 °C. The coupling reagent configuration was reagent A, reagent B, reagent C and BPA with a volume ratio of 1:1:1:2. Then, 5 mg of MoS_2/ZnO powder was dissolved in 10 mL alcohol for subsequent detection. Then the coupling agent 25 μL and an equal amount of the solution were dropped into the aluminum plate for the subsequent test. All SERS signals were detected by a Renishaw inVia Raman system under a 514.5 nm Ar^+ ion laser, the laser power is 80 mW, attenuating 50%, 30 s exposure time and 2 scan every spectrum.

The SERS experiments of BPA in the water samples

In order to avoid other factors interfering, we pretreated the water samples with membrane filters (0.45 μm and 0.22 μm) before detecting BPA in actual water samples. The test process is consistent with above.

Results and discussion

Characterization analysis of MoS_2/ZnO MCs

Scheme 1 illustrates the growth flow diagram of MoS_2/ZnO MCs. The XRD spectra of the MoS_2 and the MoS_2/ZnO are shown in Fig. 1a. The crystal structures of the MoS_2 sample were clarified to be the pure hexagonal phases of MoS_2. The

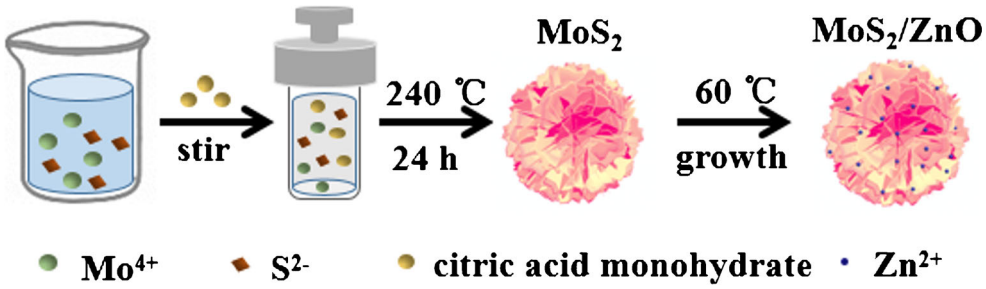

Scheme 1 Schematic illustrations of the low-cost synthesis procedure to obtain MoS_2/ZnO MCs

MoS_2 displays seven main diffraction peaks at 2θ = 14.38°, 29.03°, 32.68°, 39.54°, 44.15°, 49.79°, and 58.33°. They can be attributed to the (002), (004), (100), (103), (006), (105) and (110) lattice planes of the 2H-MoS_2 (JCPDS card No. 37–1492) crystal characteristics, respectively. In addition, the strongest peak at 2θ = 14.38° indicates that the MoS_2 has good laminar growth in the c-axis direction. As shown in the MoS_2/ZnO samples, all the diffraction peaks are indexed to the hexagonal phase (JCPDS card No. 36–1451). And the diffraction peaks appeared at 2θ = 31.76°, 34.51°, 36.23°, 47.63°, 56.58°, 62.78°, 67.82° and 69.11° can be assigned to the (100), (002), (101), (102), (110), (103), (112) and (201) lattice planes of hexagonal ZnO, respectively. The XRD pattern of MoS_2/ZnO MCs exactly corresponds to the lattice planes of ZnO and MoS_2, which indicates that the inherent structure of each component is perfectly retained during the reaction.

XPS was used to investigate the chemical states of Mo, S, Zn and O in MoS_2/ZnO MCs. The survey scan spectra of MoS_2/ZnO MCs and MoS_2 MFs have been presented in Fig. 1b, which confirms the presence of constituent elements in each compound. As shown in Fig. 1c, binding energies for Mo $3d_{3/2}$, Mo $3d_{5/2}$ are fitted to 231.29 eV and 228.13 eV, respectively, which confirms the dominance of Mo^{4+} accordingly. After forming MoS_2/ZnO MCs, these two characteristic peaks shift to 228.47 eV and 231.78 eV. The other two peaks correspond to 232.72 eV and 235.92 eV, respectively, which are characteristic of the Mo^{6+} oxidation state. The emergence of Mo^{6+} is due to the combination of Mo with O in ZnO during the formation of the MoS_2/ZnO MCs, which indicates that the oxidation reaction occurred during the hybridization process [19]. A small lower energy peak at 225.75 eV can be found, which is attributed to the S 2 s orbital of sulfide ions. As shown in Fig. 1d, peaks are observed at 160.96 and 162.13 eV due to the S $2p_{3/2}$ and S $2p_{1/2}$ of pristine MoS_2 MFs [20]. Compared to those of pristine MoS_2 MFs, the doublet peaks of S 2p of the MoS_2/ZnO MCs show a blue shift again. In the MoS_2/ZnO MCs, the small shifts in binding energy for Mo 3d and S 2p electrons directly show the charge or energy transfer between MoS_2 and ZnO caused by close contact in the heterojunction. Figure 1e shows two peaks at 1021.06 eV

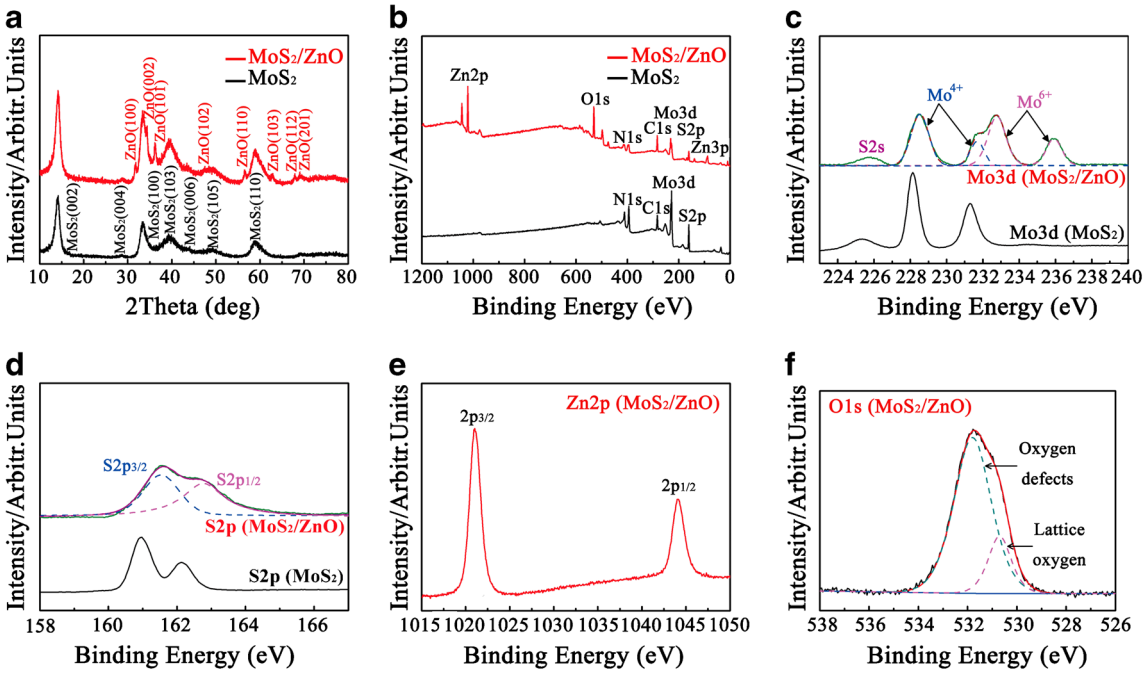

Fig. 1 **a** X-ray diffraction patterns for MoS_2 MFs and MoS_2/ZnO MCs; X-ray photoelectron spectra (XPS) for **b** Survey spectrum (MoS_2 and MoS_2/ZnO); **c** Mo-3d; **d** S-2p; **e** Zn-2p; **f** O-1

and 1044.07 eV, which corresponds to the Zn $2p_{3/2}$ and Zn $2p_{1/2}$ of MoS_2/ZnO MCs, indicating the +2-valence state of the Zn element [21]. In addition, the O 1 s signal can also be divided into two peaks, corresponding to different oxygen species. Figure 1f is the XPS spectrum of O 1 s, where the peak at 530.68 eV is associated with the O^{2-} ions in the metal oxide attributed to the lattice oxygen, while the other peak located at 531.80 eV is attributed to the O^{2-} ions in the oxygen-deficient regions [22].

The morphologies of synthesized MoS_2 MFs and MoS_2/ZnO MCs are presented in Fig. 2. As shown in Fig. 2a and b, the pristine MoS_2 samples are actually flower-like microspheres with the diameters of about ~3–5 μm. Large free spaces are shown in the layered hierarchical structure, which allows for further modification with ZnO NPs. In Fig. 2e and f, it is shown that ZnO NPs are scattered over the surfaces of the MoS_2 MFs. Furthermore, TEM images of these samples were taken to further investigate morphologies and nanostructures. It can be clearly observed in Fig. 2c that the folds of MoS_2 MFs are very thin and overlap with each other, forming the flower-like structure. The high-resolution transmission electron microscopy (HRTEM) image in the Fig. 2d shows that the lattice spacing was 0.62 nm, which maintains the theoretical spacing in the (002) planes of hexagonal MoS_2 structure [23]. Figure 2g shows a typical TEM image of MoS_2/ZnO MCs. The MoS_2 MFs were dotted with many ZnO NPs, ranging in size from 16 to 25 nm. The representative HRTEM image in Fig. 2 h, which clearly shows the deposited ZnO NPs with particle size of approximately 20 nm. It is observed that the d-spacing is 0.26 nm for the lattice fringes of ZnO, corresponding to the (001) lattice plane of hexagonal ZnO [24]. In the MoS_2/ZnO MCs, we also find the lattice spacing is 0.62 nm for the (002) plane of the hexagonal MoS_2. More importantly, the intimate interface between MoS_2 MFs and ZnO NPs is clearly observed, implying the formation of the heterojunction between these two components. The areas in different colors in Fig. 2i-l correspond to Mo, S, Zn, and O in the MoS_2/ZnO, respectively, which proves that the elements were homogeneously distributed.

SERS enhancement of MoS_2/ZnO MCs for trace bisphenol a detection

To validate the excellent SERS activity and low detection limits of the MoS_2/ZnO substrates, the SERS spectra of BPA with various concentrations from 10^{-4} M to 10^{-9} M are shown in the Fig. 3a. In this work, we found that the intensity of the SERS peak at 1592 cm^{-1} shows a correlation with the concentration of BPA and can be further used for quantitative analysis of BPA. Furthermore, the results show that the intensity of the Raman spectral bands decreased with a decrease in the concentration of BPA. An exciting result was that characteristic peaks of BPA were still distinguishable as low as 10^{-9} M, demonstrating the high sensitivity of the MoS_2/ZnO MCs. It is interesting to note that the SERS spectra at BPA concentrations of 10^{-4} M differ from several other spectra with SERS nanoprobe characteristic peaks at ~1048 and 1070 cm^{-1}. This is because the high concentration of the probe

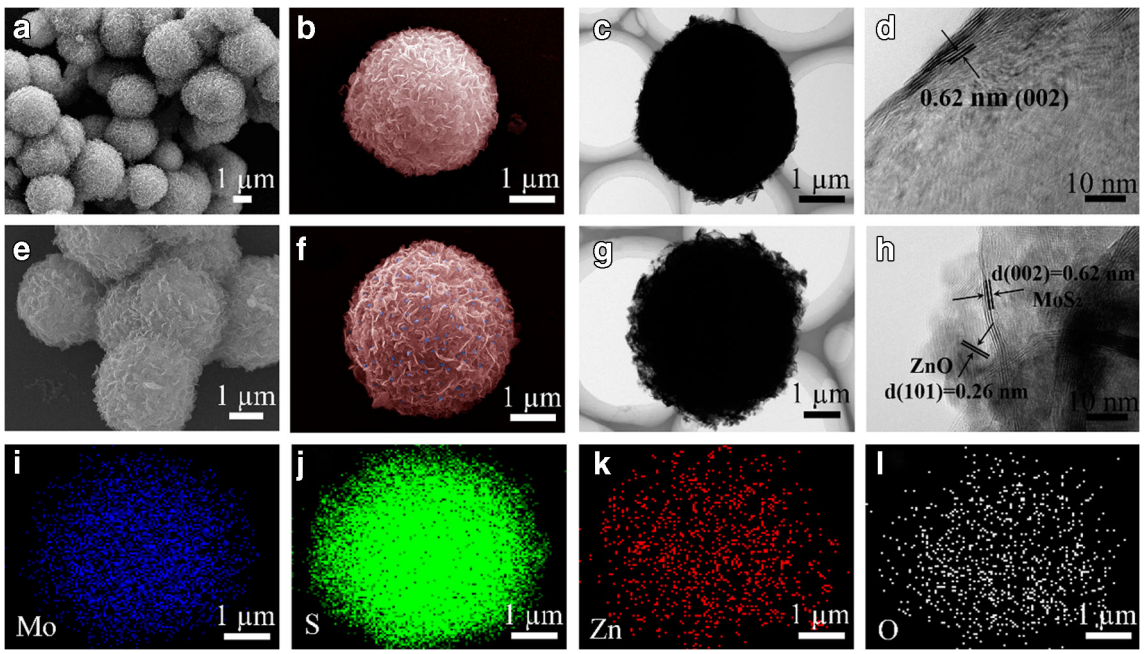

Fig. 2 **a** and **b** are SEM images of the MoS_2 MFs in different magnification; **c** TEM image of a typical MoS_2 MFs; **d** HRTEM image of MoS_2 MFs; **e** and **f** are SEM images of the MoS_2/ZnO MCs in different magnification; **g** TEM image of a typical MoS_2/ZnO; **h** HRTEM image of MoS_2/ZnO MCs; **i-l** The elemental mapping of Mo, S, Zn, O of MoS_2/ZnO MCs, respectively

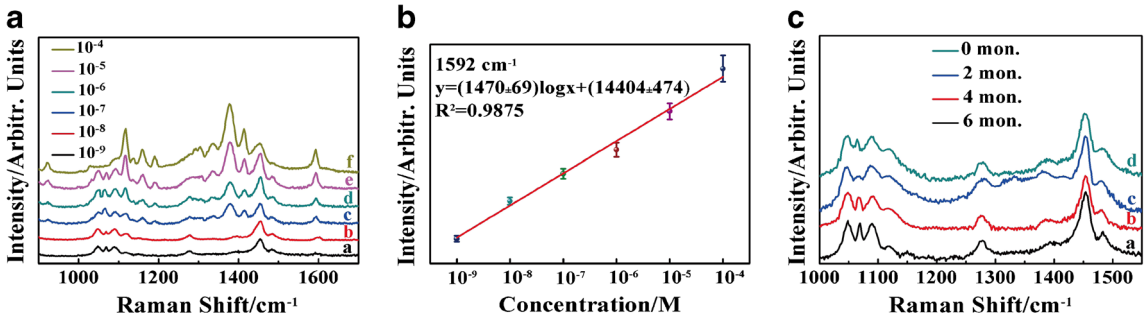

Fig. 3 **a** SERS spectra of MoS_2/ZnO MCs incubated with BPA solution at various concentration; **b** the calibration plot for BPA at 1592 cm^{-1}; **c** SERS spectra of BPA aqueous solution at 10^{-9} M based on MoS_2/ZnO collected at different shelf time

inhibited the SERS response of the coupling agent. Subsequently, the decrease in BPA concentration resulted in a spike in the probe [25]. In addition, to get statistically meaningful results, 10 points of SERS spectra were randomly collected for each concentration. And relative standard deviations (RSD) of different concentrations were calculated based on the 10 different points for the same band at 1592 cm^{-1}, as shown in Fig. 3b. The linear equation can be described as:

$$\log(I_{1592}) = (14404 \pm 474) + (1470 \pm 69)\log C_{BPA}$$

with a squared correlation coefficient of $R^2 = 0.9875$. This value (1 pM) is about 1000 times lower than the no effect concentration (PNEC) values of potable water defined by the US EPA as 0.6 to 7.0 nM (bisphenol A Action Plan, 2010).

The enhancement factor (EF) was calculated by the following equation [26, 27]:

$$\mathrm{EF} = \left(\frac{I_{SERS}}{I_{Raman}}\right)\left(\frac{N_{Raman}}{N_{SERS}}\right)$$

Where I is the corresponding intensity of the line selected and N is the number of BPA molecules sampled by the laser spot. N_{SERS} is 1.51×10^{19} and N_{Raman} is 7.82×10^{23}. The in-plane at 1592 cm^{-1} was chosen for calculation of the EF. We obtain for the ratio of intensities I_{SERS} / I_{Raman} = 6073/542 = 11.2. The EF was estimated to be 5.8×10^5. As far as we know, the SERS performance of MoS_2/ZnO MCs is superior to that of previously reported semiconductor nanomaterials. In practical applications, the stability of the SERS substrates is another significant factor that must be considered. As shown in Fig. 3c, it is observed that the peak strength of the BPA peaks at 1592 cm^{-1} was almost unchanged with an increase in time, which indicated the extremely high stability of the MoS_2/ZnO MCs substrate. These results demonstrated that the MoS_2/ZnO MCs were effective in forming a stable SERS substrate that can be stored long-term under ambient conditions. Therefore, MoS_2/ZnO MCs can be widely applied in food analysis, environmental monitoring, SERS tags and other practical applications [28].

SERS analysis of BPA residue in the water samples

Water samples were taken from local tap water. Figure 4a shows 10 randomly selected positions on the MoS_2/ZnO MCs substrate. As shown in Fig. 4b, the calculated RSD of the intensities of the peaks at 1592 cm^{-1} were 7.5%, which indicating great reproducibility of the MoS_2/ZnO MCs substrate. According to the linear equation, the BPA residue in water samples is calculated to be 5.6×10^{-9} mol·L^{-1}, which is far below the maximum BPA concentration of 1×10^{-5} g·L^{-1} in the tap water according to the Chinese National Standard. On the other hand, these SERS spectra also show that MoS_2/ZnO MCs SERS substrate has extremely high uniformity.

Mechanism of SERS detection

Normally, electromagnetic mechanisms (EM) and chemical mechanisms (CM) are widely recognized as SERS enhancement mechanisms. In our experiment, the SERS intensity of the hybrid structure was higher than that of the individual component, which are dominated by the CM rather than the EM as the EM is the dominant mechanism of metals used as SERS substrates [29–33]. However, traditional CT process enhancement in SERS fall in the range between 10^1 and 10^3 lower than the calculated EF (5.8×10^5). Thus, a potential enhancement mechanism should be responsible for the outstanding SERS. When ZnO NPs are deposited onto the surface of the MoS_2 MFs, an efficient interface between ZnO and MoS_2 is formed. Due to the different band gaps of ZnO and MoS_2, the photo-induced electrons on the conduction band (CB) of MoS_2 would migrate to the CB of ZnO. The photo-induced holes would migrate to the valence band (VB) of MoS_2 from the VB of ZnO. Driven by the interfacial electronically filed the photoelectrons of ZnO in the CB can be rapidly transferred to the VB of MoS_2, thus inhibiting the recombination of photo-induced carriers in the component, respectively. Therefore, the photo-induced holes will remain on the CB of ZnO and the photoelectrons will exist in the VB of MoS_2. As

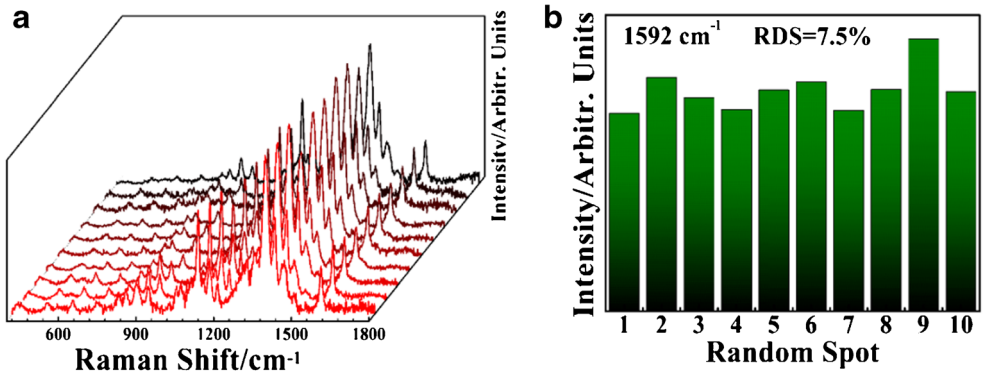

Fig. 4 **a** a series of SERS spectra of BPA in water samples collected on 10 randomly selected spots of the MoS_2/ZnO MCs substrate; **b** SERS intensity of BPA at 1592 cm^{-1} of the 10 SERS spectra

shown by the horizontal dashed line in Scheme 2, a unified Fermi energy level (EF) is established at the heterojunction at the thermal equilibrium. In addition, the transfer of the initial charge carrier at the junction contact gives rise to the depletion regions, yielding internal electric fields and inducing band bending at the interface. As a result, the occurrences of the electrons transmission processes yield a substrate effective for SERS. In addition, oxygen vacancy may play an irreplaceable role in enriching the surface states of semiconductor to provide magnified affinity for the adsorbent-adsorbate interaction, which results in a further increase to the SERS signals through CT process. Providing with efficient charge transfer processes between the matching energy levels of adsorbed probe molecules and the semiconductor, both the polarizability tensor and the electron density distribution of the molecule would be modified, leading to the observation of non-totally symmetric SERS modes. As shown in Scheme 2, oxygen vacancy-associated electronic state (V_O) well separated from the bottom of the CB. It can be expected that contributions from several types of thermodynamically feasible CT resonance may be related to the overall Raman enhancement in our MoS_2/ZnO MCs-BPA system at an excitation of 514.5 nm, including exciton resonance of MoS_2/ZnO MCs defect states, and the photon induced CT resonance from matched energy level between MoS_2/ZnO MCs and BPA molecules. These resonances will lead to a magnification of Raman scattering cross-section. Moreover, we believe another reason for the SERS enhancement was thought to the semiconducting property of MoS_2, because it has sulfur atoms on its surface as well as a polar covalent bond (Mo-S) with the polarity in the vertical direction to the surface [34]. In summary, the both charge transfer and dipole-dipole coupling can significantly enhance the intensity of Raman spectroscopy.

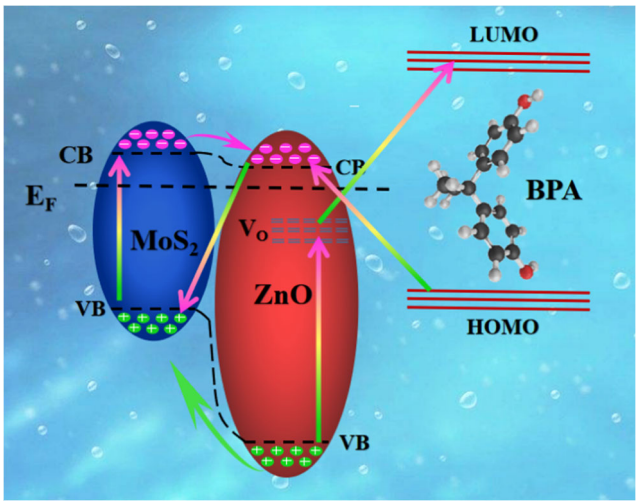

Scheme 2 Schematic illustration of the SERS mechanism of MoS_2/ZnO MCs

Conclusion

It is the first time that MoS_2/ZnO MCs served as SERS-active substrates for the trace detection of BPA, with the detection limits as low as 1×10^{-9} M. ZnO NPs are uniformly distributed on the surface of MoS_2 MFs, resulting in a larger specific surface area. In addition, because of the special band characteristics of MoS_2 and ZnO, the heterojunctions were constructed between them which have stronger charge transfer capabilities. Our study broke through the application barrier of semiconductor composite materials in SERS substrates, which lays a foundation for the rapid detection of bisphenol compounds in food containers, industrial and clinical samples. In addition, optimizing the time-consuming problem of the experimental scheme will be our next research focus.

Acknowledgements This work is supported by the National Natural Science Foundation of China (No. 61675090, 61575080, 61705020 and 21676115); National Youth Program Foundation of China (No. 61405072, 21546013, 61704065, 61705078 and 51609100); Program for the development of Science and Technology Jilin province (Grant Numbers 20160101287JC and 20150519024JH); and Technology of Education Department of Jilin Province (Grant Number JJKH20170374KJ).

Compliance with ethical standards The author(s) declare that they have no competing interests.

References

1. Yin D, Chen YL, Zhang YH, Yang ZC, Mao HY, Xia SG, Zhang WF, Zhao WD, Zhang SS (2018) 2D porous aromatic framework as a novel solid-phase extraction adsorbent for the determination of trace BPA in Milk. Microchim Acta 81(5):749–758. https://doi.org/10.1007/s10337-018-3504-6
2. Liu Y, Chen Y, Zhang YY, Kou QW, Zhang YJ, Wang YX, Chen L, Sun YT, Zhang HL, Jung YM (2018) Detection and identification of estrogen based on surface-enhanced resonance Raman scattering (SERRS). Molecules 23(6):1330. https://doi.org/10.3390/molecules23061330
3. Liang LP, Zhang J, Feng P, Li C, Huang YY, Dong BZ, Li LN, Guan XH (2015) Occurrence of bisphenol a in surface and drinking waters and its physicochemical removal technologies. Microchim Acta 9(1):16–38. https://doi.org/10.1007/s11783-014-0697-2
4. Xu JY, Li Y, Bie JX, Jiang W, Guo JJ, Luo YL, Shen F, Sun CY (2015) Colorimetric method for determination of bisphenol a based on aptamer-mediated aggregation of positively charged gold nanoparticles. Microchim Acta 182(13):2131–2138. https://doi.org/10.1007/s00604-015-1547-z
5. Gatidou G, Thomaidis NS, Stasinakis AS, Lekkas TD (2007) Simultaneous determination of the endocrine disrupting compounds nonylphenol, nonylphenol ethoxylates, triclosan and bisphenol a in wastewater and sewage sludge by gas chromatography-mass spectrometry. J Chromatogr A 1138(1):32–41. https://doi.org/10.1016/j.chroma.2006.10.037
6. Wu XQ, Wang XY, Lu WH, Wang XR, Li JH, You HY, Xiong H, Chen LX (2016) Water-compatible temperature and magnetic dual-responsive molecularly imprinted polymers for recognition and extraction of bisphenol a. J Chromatogr A 1435(26):30–38. https://doi.org/10.1016/j.chroma.2016.01.040
7. Shorie M, Kumar V, Kaur H, Singh K, Tomer VK, Sabherwal P (2018) Plasmonic DNA hotspots made from tungsten disulfide nanosheets and gold nanoparticles for ultrasensitive aptamer-based SERS detection of myoglobin. Microchim Acta 185:158. https://doi.org/10.1007/s00604-018-2705-x
8. Qian Y, Wang YQ, Mei RC, Yin YC, You JM, Chen LX (2019) Polystyrene encapsulated SERS tags as promising standard tools: simple and universal in synthesis, highly sensitive and Ultrastable for bioimaging. Anal Chem 91(8):5270–5277. https://doi.org/10.1021/acs.analchem.9b00038
9. Wang YQ, Yan B, Chen LX (2013) SERS tags: novel optical Nanoprobes for bioanalysis. Chem Rev 113(3):1391–1428. https://doi.org/10.1021/cr300120g
10. Ren XH, Cheshari EC, Qi JY, Li X (2018) Silver microspheres coated with a molecularly imprinted polymer as a SERS substrate for sensitive detection of bisphenol a. Microchim Acta 185(4):242. https://doi.org/10.1007/s00604-018-2772-z
11. Wang XT, Shi WX, Wang SX, Zhao HW, Lin J, Yang Z, Chen M, Guo L (2019) Two-Dimensional Amorphous TiO_2 Nanosheets Enabling High-Efficiency Photoinduced Charge Transfer for Excellent SERS Activity. J Am Chem Soc 141(14):5856–5862. https://doi.org/10.1021/jacs.9b00029
12. Noh T, Shin HS, Seo C, Kim JY, Youn J, Kim J, Lee KS, Joo J (2019) Significant enhancement of photoresponsive characteristics and mobility of MoS_2-based transistors through hybridization with perovskite $CsPbBr_3$ quantum dots. Microchim Acta 12:405–412. https://doi.org/10.1007/s12274-018-2230-6
13. Wu W, Wang L, Li Y, Zhang F, Lin L, Niu S, Chenet D, Zhang X, Hao Y, Heinz TF, Hone J, Wang ZL (2014) Piezoelectricity of single-atomic-layer MoS_2 for energy conversion and piezotronics. Nature 514(7523):470–474. https://doi.org/10.1038/nature13792
14. Vilian ATE, Dinesh B, Kang SM, Krishnan M, Huh YS, Han YK (2019) Recent advances in molybdenum disulfide-based electrode materials for electroanalytical applications. Microchim Acta 186(3):203. https://doi.org/10.1007/s00604-019-3287-y
15. Zhao XF, Yu J, Zhang ZJ, Li CH, Li Z, Jiang SZ, Pan J, Liu AH, Zhang C, Man BY (2018) Heterogeneous and cross-distributed metal structure hybridized with MoS_2 as high-performance flexible SERS substrate. Opt Express 26(18):23831–23843. https://doi.org/10.1364/OE.26.023831
16. Yao JC, Quan YN, Gao M, Gao RX, Chen L, Liu Y, Lang JH, Shen H, Zhang YJ, Yang LL, Yang JH (2019) AgNPs decorated mg-doped ZnO Heterostructure with dramatic SERS activity for trace detection food contaminants. J Mater Chem C 7:8199–8208. https://doi.org/10.1039/C8TC06588H
17. Nur HH, Shanmugam S, Mutharasu D, Abdul RI (2016) Structural and surface characterization of undoped ZnO and cu doped ZnO using sol–gel spin coating method. Microchim Acta 27(4):3520–3530. https://doi.org/10.1007/s10854-015-4187-5
18. Gao M, Yan C, Li BZ, Zhou LJ, Yao JC, Zhang YJ, Liu HL, Cao LH, Cao YT, Yang JH, Wang YX (2017) Strong red emission and catalytic properties of ZnO by adding Eu2O3 shell. J Alloys Compd 724(15):537–542. https://doi.org/10.1016/j.jallcom.2017.07.060
19. Islam SE, Hang DR, Chen CH, Sharma KH (2018) Facile and cost-efficient synthesis of quasi 0D/2D ZnO/MoS_2 nanocomposites for highly enhanced visible-light-driven photocatalytic degradation of organic pollutants and antibiotic. Chemistry 24(37):9305–9315. https://doi.org/10.1002/chem.201801397
20. Kibsgaard J, Chen Z, Reinecke BN, Jaramillo TF (2012) Engineering the surface structure of MoS_2 to preferentially expose active edge sites for electrocatalysis. Nat Mater 11(11):963–969. https://doi.org/10.1038/nmat3439
21. Gao M, Yao JC, Yan C, Li XF, Hu TJ, Chen L, Wang YX, Zhang YJ, Liu HL, Liu Y, Cao LH, Cao YT, Yang JH (2017) Novel composite nanomaterials with superior thermal and pressurestability for potential LED applications. J Alloys Compd 734(15):282–289. https://doi.org/10.1016/j.jallcom.2017.11.042
22. Zheng ZH, Cong S, Gong W, Xuan J, Li G, Lu W, Geng F, Zhao Z (2017) Semiconductor SERS enhancement enabled by oxygen incorporation. Nat Commun 8(1):1993. https://doi.org/10.1038/s41467-017-02166-z
23. Tan YH, Yu K, Li JZ, Fu H, Zhu ZQ (2014) MoS_2@ZnO nanoheterojunctions with enhanced photocatalysis and field emission properties. J Appl Phys 116(6):064305. https://doi.org/10.1063/1.4893020
24. Bang S, Lee S, Ko Y, Park J, Shin S, Seo H, Jeon H (2012) Photocurrent detection of chemically tuned hierarchical ZnO nanostructures grown on seed layers formed by atomic layer deposition. Nanoscale Res Lett 7(1):290. https://doi.org/10.1186/1556-276X-7-290
25. Marks HL, Pishko MV, Jackson GW, Cote GL (2014) Rational design of a bisphenol a aptamer selective surface enhanced raman scattering nanoprobe. Anal Chem 86(23):11614–11619. https://doi.org/10.1021/ac502541v
26. Moeinian A, Gür FN, Gonzalez-Torres J, Zhou LS, Murugesan VD, Dashtestani AD, Guo H, Schmidt TL, Strehle S (2019) Highly localized SERS measurements using single silicon nanowires decorated with DNA origami-based SERS probe. Nano Lett 19(2):1061–1066. https://doi.org/10.1021/acs.nanolett.8b04355
27. Yao JC, Quan YN, Gao RX, Li J, Chen L, Liu Y, Lang JH, Shen H, Wang YY, Yang JH, Gao M (2019) Improved charge-transfer and hot spots by doping and modulating semiconductor structure: a high sensitivity and renewability SERS substrate. Langmuir 35:8921–8926. https://doi.org/10.1021/acs.langmuir.9b00754

28. Mei RC, Wang YQ, Liu WH, Chen LX (2018) Lipid bilayer-enabled synthesis of waxberry-like Core/fluidic satellite nanoparticles: toward ultrasensitive SERS tags for bioimaging. ACS Appl Mater Interfaces 10(28):23605–23616. https://doi.org/10.1021/acsami.8b06253
29. Balčytis A, Nishijima Y, Krishnamoorthy S, Kuchmizhak A, Stoddart PR, Petruškevičius R, Juodkazis S (2018) From fundamental toward applied SERS: shared principles and divergent approaches. Adv Opt Mater 6(16):1800292. https://doi.org/10.1002/adom.201800292
30. Zhang XY, Han DL, Ma N, Gao RX, Zhu AN, Guo S, Zhang YJ, Wang YX, Yang JH, Chen L (2018) Carrier density-dependent localized surface Plasmon resonance and charge transfer observed by controllable semiconductor content. J Phys Chem Lett 9(20):6047–6051. https://doi.org/10.1021/acs.jpclett.8b02416
31. Gao RX, Zhang YJ, Zhang F, Guo S, Wang YX, Chen L, Yang JH (2018) SERS polarization-dependent effects for an ordered 3D Plasmonic tilted silver Nanorod array. Nanoscale 10:8106–8114. https://doi.org/10.1039/C8NR01198B
32. Zhang YJ, Sun HH, Gao RX, Zhang F, Zhu AN, Chen L, Wang YX (2018) Facile SERS-active chip (PS@ag/SiO_2/ag) for the determination of HCC biomarker. Sensors Actuators B Chem 272(1):34–42. https://doi.org/10.1016/j.snb.2018.05.139
33. Yang LY, Fu CC, Wang HL, Xu SP, Xu WQ (2016) Aptamer-based surface-enhanced Raman scattering (SERS) sensor for thrombin based on supramolecular recognition, oriented assembly, and local field coupling. Microchim Acta 409(1):235–242. https://doi.org/10.1007/s00216-016-9992z
34. Ling X, Fang W, Lee YH, Araujo PT, Zhang X, Rodriguez-Nieva JF, Lin Y, Zhang J, Kong J, Dresselhaus MS (2014) Raman enhancement effect on two-dimensional layered materials: graphene, h-BN and MoS_2. Nano Lett 14(6):3033–3040. https://doi.org/10.1021/nl404610c